Line Shapes and Configuration Interaction of Exciton Resonances*†

K. P. JAIN
Department of Physics and Institute for the Study of Metals, University of Chicago, Chicago, Illinois
(Received 7 January 1965)

To describe optical absorption in insulators and semiconductors the random-phase-approximation formulation of the dielectric response is extended to include resonant as well as scattering states. Characteristic interference effects are obtained within this generalized random-phase approximation for exciton resonances both above and below the direct absorption threshold, and these give rise to intrinsic asymmetries in the line shapes. The absorption is described in terms of a collective phase shift Δ and the electron-hole scattering channels $\Omega_{ll'}$. In the presence of Raman (interband) scattering the collective phase shift becomes complex. As an example the ultraviolet absorption spectrum of solid xenon, as measured by Baldini, is analyzed. Theoretical line shapes are in good agreement with the experimental ones. Configuration interaction between families of resonances is invoked to explain the anomalies in the binding energies and oscillator strengths of $\Gamma(\frac{1}{2})$ and $L(\frac{3}{2})$ excitons in solid xenon.

1. INTRODUCTION

BELOW the direct absorption threshold, the line absorption associated with hydrogenic excitons is well known.[1] There are two different approaches[2,3] to the theory of line shapes of these exciton bands. Both are concerned with the effect of exciton-phonon interactions on the line shape. In the Toyozawa[2] approach the line shape of an isolated resonance, in the weak-coupling limit, due to the phonon-induced exciton decay is a symmetric Lorentzian with a decay width γ_α, where α labels the resonance in question. Nearby exciton absorption bands cause an asymmetry in this Lorentzian peak accompanied by an antiresonance which subtracts from the background intensity. Elliott[3] has discussed the indirect (phonon-assisted) exciton formation with the use of second-order perturbation theory. Again the line shape is Lorentzian with a corresponding width.

We are concerned here with the more general problem of exciton resonances which may lie either above[4] or below the direct absorption threshold. For an isolated resonance in the fundamental region there are two basic contributions to decay processes. Firstly there is the intrinsic contribution corresponding to the coherent exciton-photon field. This results in autoionization of the exciton with a width Γ_α. Secondly there is the extrinsic contribution due to the incoherent exciton-phonon field resulting in phonon-induced decays with width γ_α.

We propose to show that the coherent exciton-exciton interaction mediated by the photon field[5] is instrumental in determining the line shapes. The asymmetry of the line shapes is similar to that discussed by Fano[6] for two-electron atomic excitations. Hence the line shape of the hydrogenic exciton resonances is rather similar to that observed in the $2s\,np$ Rydberg series of atomic He and may be described in terms of a collective phase shift Δ. However, the difference between the two is that in the atomic case instrumental and collision broadening effects can be made quite small, so that $\gamma_\alpha \ll \Gamma_\alpha$, but in the crystalline case, defect and phonon scattering make $\gamma_\alpha \gtrsim \Gamma_\alpha$.

Interference effects between coherent resonances and interband scattering in the fundamental absorption region have been invoked to explain the line-shape anomalies in this region of the spectra of insulators and semiconductors.[7] Here we wish to discuss the effects that are obtained when one or more families of coherent resonances overlap one or more interband absorption continua.

In Sec. 2 the linear dielectric response of a many-body system containing only quasiparticle and transverse coherent excitations (excitons) is described in terms of a generalized random phase approximation[8–11] (GRPA). In so doing it is found that each pair of electron-hole bands generates a distinct channel for its own family of coherent resonances. If the resonances belonging to a family interact with each other through second-order interactions by autoionization into their parent channel, then this corresponds to the GRPA. Within the GRPA no interference effects are expected on the proper self-energies of resonances belonging to predominantly different channels. Configuration interaction among the different families, corresponding to interband mixing, is shown in Sec. 3 to be equivalent to a partial breakdown of the GRPA. When the quasiparticle band structure is well understood, it is then possible to identify the effects of configuration interaction on the real part of exciton-photon proper self-energies. One of the effects of breakdown of the GRPA is to cause Raman decay of

* This work was supported by the NSF and NASA.
† Presented as a thesis to the Department of Physics, University of Chicago, in partial fulfillment of the requirements for the Ph.D. degree.
[1] R. S. Knox, *Theory of Excitons, Solid State Physics, Suppl. 5* (Academic Press, Inc., New York, 1963).
[2] Y. Toyozawa, Progr. Theoret. Phys. (Kyoto) **20**, 53 (1958).
[3] R. J. Elliott, in *Proceedings of International Conference on Semiconductor Physics* (Czechoslovak Academy of Sciences, Prague, 1961), p. 408.
[4] J. C. Phillips, Phys. Rev. **136**, A1705 (1964).
[5] J. C. Phillips, Phys. Rev. **136**, A1714 (1964).
[6] U. Fano, Phys. Rev. **124**, 1866 (1961).
[7] J. C. Phillips, Phys. Rev. Letters **12**, 447 (1964).
[8] H. Ehrenreich and M. H. Cohen, Phys. Rev. **115**, 786 (1959).
[9] S. L. Adler, Phys. Rev. **126**, 413 (1962).
[10] P. Nozières and D. Pines, Phys. Rev. **109**, 762 (1958).
[11] P. Nozières and D. Pines, Nuovo Cimento **9**, 470 (1958).

an exciton resonance into another resonance belonging to a different channel with the emission of a photon corresponding to the energy difference between the two exciton states. The collective phase shift belonging to this channel becomes complex—the imaginary part corresponding to the imaginary part of the exciton-photon self-energies. In order to maintain the identity of a phase shift belonging to a given channel it is necessary to assume that resonances belonging to separate channels do not overlap too strongly. Within the framework of perturbation theory a consistent expression can be obtained for the linear dielectric response of the system.

So far we have discussed interference effects in the fundamental absorption region. Below the absorption threshold oscillator strengths and line shapes near the series limit have been discussed by Elliott.[12] The intrinsic spectrum here at $T=0$ represents transitions only to bound pair states. In the presence of defects or phonons, background absorption into scattering states is also found. Again interference between the resonant and background absorption causes an asymmetry in the line shape of the coherent resonances.

Toyozawa,[13] considering transitions only to resonant states, used second-order perturbation theory to calculate the effect of phonons on the exciton spectra. In this the interference terms coming from a pair of different intermediate states were rearranged so that each resonance becomes asymmetric and the so-called intensity additivity rule was obtained.

Hopfield[14] has criticized Toyozawa's approach on the grounds that to compute the absorption spectrum one should add *amplitudes*, not intensities. Our GRPA formulates Hopfield's viewpoint in a manner suited to quantitative calculation. Hence a by-product of our viewpoint is an internally consistent approach to the asymmetries of resonances not only above but also below the direct absorption threshold.

Section 2 presents a formulation of the dielectric response of a many-electron system containing quasiparticles and coherent pair resonances. The Fano formalism is then invoked to describe the resonance behavior of this many-body system within the GRPA. A single-channel approximation is made, corresponding to which the collective phase shift is wholly real. Section 3 extends the theory to include the breakdown of the GRPA resulting from the configuration interaction of collective resonances belonging to two separate channels. On making the Van Kampen[15] ansatz the collective phase shifts of the separate channels become complex. Linear combinations of the degenerate scattering states belonging to the two channels are taken to describe the eigenmodes of the system and an expression is obtained for the dielectric response. Section 4 describes the manner in which the line shapes can be generated according to the theory. The effect of the phonons is taken into account by folding the line shapes with an energy-dependent Gaussian parameter $\gamma(E)$. The line shapes depend on the ratio $\gamma_\alpha/\Gamma_\alpha$ and q_α where Γ_α is the autoionization rate and q_α is the amplitude strength of the resonance in question. Kramers-Kronig transforms are taken to obtain the absorption coefficient $\mu(E)$ from $\epsilon_2(E)$. The choice of the background density of states is also discussed.

As an example we discuss in Sec. 5 the ultraviolet absorption spectrum of solid Xe measured by Baldini.[16] The line shapes are examined in the single-channel, two independent channels, and two mixed channels approximations. The optimum values of parameters γ, Γ, q, W are determined where W^2 is the Raman decay rate. An estimate is made of the ratio between interband and intraband scattering matrix elements, and the theoretical line shapes are compared to the experimental ones of Baldini. Section 6 discusses configuration interaction in xenon.

2. GENERALIZED RANDOM-PHASE APPROXIMATION

The linear dielectric response of a many-body system containing only scattering (quasiparticle) excitations and longitudinal collective (plasma) excitations has been discussed in many papers.[8–11] In most cases the random-phase approximation (RPA) is made which is equivalent to the Hartree or Hartree-Fock approximation for the quasiparticle excitations

$$\epsilon(k,\omega)=1-\lim_{\alpha\to 0+}\frac{4\pi e^2}{m^2\omega^2 V}\sum_{k',l'}|\langle \mathbf{k}'l'|T|\mathbf{k}+\mathbf{k}',l'\rangle|^2 \times\frac{f_0(E_{k+k',l'})-f_0(E_{k',l})}{E_{k+k',l'}-E_{k'l}-\hbar\omega+i\alpha}. \quad (1)$$

It is a straightforward matter to extend the treatment to include transverse coherent excitons. We generalize (1) by writing it in the form

$$\epsilon(k,\omega)=1-\lim_{\alpha\to 0+}\frac{4\pi e^2}{m^2\omega^2 V}\sum_{i,f}\frac{|\langle f,\mathbf{k}|T|i,0\rangle|^2}{E_f-E_i-\hbar\omega+i\alpha} \quad (2)$$

where T is the electric-dipole transition operator between i and f, the initial and final states, respectively. The final state $|f,\mathbf{k}\rangle$ contains as one of its terms the exciton amplitude. Using the Wannier model, the exciton eigenstate may be written from translational symmetry[12,17]

$$\phi_k^{ll'}(\mathbf{r}_1,\mathbf{r}_2)=\exp[\tfrac{1}{2}i\mathbf{k}\cdot(\mathbf{r}_1+\mathbf{r}_2)]b_{k,ll'}^{\dagger}(\mathbf{r}_1-\mathbf{r}_2)|0\rangle \quad (3)$$

[12] R. J. Elliott, Phys. Rev. **108**, 1384 (1957).
[13] Y. Toyozawa, J. Phys. Chem. Solids **25**, 59 (1964).
[14] J. J. Hopfield, J. Phys. Chem. Solids **22**, 63 (1961).
[15] N. V. Van Kampen, Kgl. Danske Videnskab. Selskab, Mat. Fys. Medd. **26**, No. 15 (1951).
[16] G. Baldini, Phys. Rev. **128**, 1562 (1962).
[17] G. Dresselhaus, J. Phys. Chem. Solids **1**, 14 (1956).

where the exciton creation operator is

$$b_{\mathbf{k},ll'}{}^{\dagger}(\mathbf{r}_1-\mathbf{r}_2) = N^{-1/2}\sum_{\mathbf{k}'}\exp[-i\mathbf{k}'\cdot(\mathbf{r}_1-\mathbf{r}_2)]C_{l,\mathbf{k}'}{}^{\dagger}C_{l',\mathbf{k}-\mathbf{k}'} \quad (4)$$

and $C_{l,\mathbf{k}}{}^{\dagger}$, $C_{l',\mathbf{k}}$ are the second-quantized electron creation (in conduction band l) and destruction (in valence band l') operators, respectively. In addition the final state contains a term corresponding to the scattering of an electron hole pair

$$\psi_{\mathbf{k},E}{}^{ll'}=\sum_{\mathbf{k}'}B_{\mathbf{k}'}C_{l,\mathbf{k}'}{}^{\dagger}C_{l',\mathbf{k}+\mathbf{k}'}|0\rangle. \quad (5)$$

The final eigenstate for one exciton state and a set of continuous scattering states corresponding to a pair of bands l, l' is

$$\Psi_{k,E}{}^{ll'}=a\phi_k{}^{ll'}(\mathbf{r}_1,\mathbf{r}_2)+\int dE'\, b_{E'}\psi_{k,E'}{}^{ll'}. \quad (6)$$

From (2)

$$\epsilon_2(k,E)=\frac{\sum_{ll'}|\langle\Psi_{k,E}{}^{ll'}|T|i\rangle|^2}{\sum_{ll'}|\langle\psi_{k,E}{}^{ll'}|T|i\rangle|^2}\epsilon_{2B}(k,E), \quad (7)$$

where $\epsilon_{2B}(k,E)$ is the imaginary part of the dielectric function due to the scattering states. In the advent of multiple exciton states (7) holds but

$$\phi_k{}^{ll'}(\mathbf{r}_1,\mathbf{r}_2) = \sum_n a_n \exp[\tfrac{1}{2}i\mathbf{k}\cdot(\mathbf{r}_1+\mathbf{r}_2)]b_{k,ll'}{}^{\dagger n}(\mathbf{r}_1-\mathbf{r}_2)|0\rangle. \quad (8)$$

Consequently (7) gives the dielectric response of a many-electron system containing quasiparticles and coherent pair resonances. From (6) it is evident that characteristic interference effects occur between the exciton and scattering eigenstates which may affect the absorption line shapes considerably.

Both above and below the direct absorption threshold there exist excitons, the scattering states for those below being provided by phonons and lattice defects. Excitons above the threshold described by $\phi_k{}^{ll'}(\mathbf{r}_1,\mathbf{r}_2)$ do not form stable bound eigenstates and may make transitions to a pair of electron-hole states ψ_{kl}, $\psi_{kl'}$ belonging to a continuum of scattering states (autoionization) by a two-electron matrix element of the form

$$\langle\psi_{kl}(\mathbf{r}_1)\psi_{kl'}(\mathbf{r}_2)|\frac{e^2}{|r_1-r_2|}|\phi^{ll'}(\mathbf{r}_1,\mathbf{r}_2)\rangle.$$

Two-electron dynamical resonances in atomic spectra have been discussed by Fano.[6] Autoionization is an elastic process and as such it is possible to use stationary eigenfunctions of the system,[15] which are linear combinations of the resonant and scattering states to describe the absorption of the photons. Consider the case of a single isolated exciton resonance described by ϕ and a single background of scattering states described by ψ_E. If the total momentum of the exciton is zero, then from (6) (suppressing the band indices)

$$\Psi_E=a\phi+\int dE' b_{E'}\psi_{E'}.$$

As expected from (7) the Lorentzian peak associated with the resonance cannot be simply superimposed on the interband scattering by the addition of intensities. On superimposing the amplitudes it is found that the resonant structure is asymmetric. If $\frac{1}{2}\Gamma$ is the half-width and E_0 the self-consistent energy of the resonant state Φ, and q is the oscillator amplitude of the resonant state relative to the scattering state, then

$$\frac{|\langle\Psi_E|T|i\rangle|^2}{|\langle\psi_E|T|i\rangle|^2}=1+\frac{q^2-1}{1+E_R{}^2}+\frac{2qE_R}{1+E_R{}^2}$$

where $E_R=2(E-E_0)/\Gamma$ and the last term represents the interference term between the resonance and scattering transitions. For $q=-E_R$, we have $\epsilon_2(E)\to 0$ and an antiresonance is obtained. The line shape is shown[6] for the above expression in Fig. 1.

On introducing a Breit-Wigner resonance phase shift Δ by $\tan\Delta=\Gamma/2(E_0-E)$ it is seen that on passing through the resonance the phase changes by π. Also in this elastic approximation the phase shift is wholly real.

Since the one-electron Hamiltonian is diagonal in the Bloch representation with the quantum numbers k and l, let us define a scattering channel $\Omega=(ll')$ as being generated from a pair of bands ll', the former filled and the latter empty of electrons. Hence, neglecting interband scattering, each channel generates its own family of resonances. If a given channel contains more than one resonance, then we get second-order interactions among exciton resonances due to each one autoionizing into the background. The coherent exciton-photon field can now be represented by the Fano equivalent Hamiltonian and it becomes necessary to diagonalize this to obtain the proper self-energies of the exciton-photon field. Let us assume that the matrix elements of the unperturbed resonant and continuum

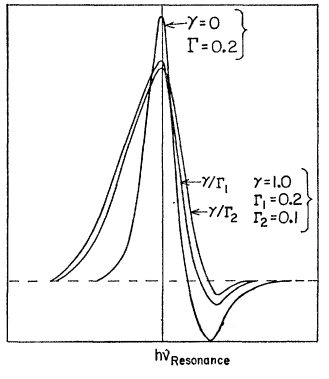

FIG. 1. Typical antiresonances for an isolated peak for $q=-5.0$ for ratios of the parameters $\gamma/\Gamma=0$, 5, 10. The dashed line represents a constant background. The antiresonance is perfect only when there are no phonon-induced decays of the exciton i.e., $\gamma=0$.

scattering states are

$$\begin{aligned}&\langle\phi_{\Lambda\Omega}|H|\phi_{n'\Omega'}\rangle=E_n\delta_{nn'}\delta_{\Omega\Omega'}\\&\langle\psi_{E\Omega}|H|\psi_{E'\Omega'}\rangle=E\delta(E-E')\delta_{\Omega\Omega'}\\&\langle\psi_{E'\Omega'}|H|\phi_{n\Omega}\rangle=V_{E'n}\delta_{\Omega\Omega'}+W_{En'}(1-\delta_{\Omega\Omega'}),\end{aligned}\tag{9}$$

where the Latin letters label the unperturbed resonances; Ω,Ω' the 2 channels; the primed and the unprimed quantities refer to channels Ω and Ω', respectively. Let us assume initially that $\Omega=\Omega'$ i.e., only one channel. Then

$$\Psi_E=\sum_n a_{n\Omega}\phi_{n\Omega}+\int dE' b_{E'\Omega}\psi_{E'\Omega}.\tag{10}$$

On calculating the eigenmodes of this system it is found that the real part of the proper self-energies of the exciton-photon field shift the energies of the resonances from E_n to E_ν. Owing to the admixture of the continuum scattering states, the half-width of the resonances are $\frac{1}{2}\Gamma_\nu$. The collective phase shift Δ_Ω of the coherent exciton-photon field belonging to the channel Ω is then

$$\tan\Delta_\Omega(E)=\sum_{\nu\epsilon\Omega}\frac{\Gamma_\nu}{2(E_\nu-E)}\equiv\sum_{\nu\epsilon\Omega}\tan\Delta_{\nu\Omega}(E)$$

and

$$\epsilon_2(E)=\cos^2\Delta_\Omega(E)\,|\sum_{\nu\epsilon\Omega}q_\nu\tan\Delta_{\nu\Omega}(E)-1\,|^2\epsilon_\Omega(E),\tag{11}$$

where $\epsilon_\Omega(E)$ is the contribution from the continuum scattering states. From (11) it is seen that there is a cross term between $\tan\Delta_1$ and $\tan\Delta_2$ etc.

We define a generalized random-phase approximation in which there is no interaction between resonances belonging to different channels and hence no interference effects on their self-energies. All the above interference effects have been obtained within the GRPA. Hence it is possible to study the line shapes generated within a single-channel approximation as is done in Sec. 5.

3. BREAKDOWN OF GENERALIZED RANDOM-PHASE APPROXIMATION AND CONFIGURATION INTERACTION

By using generalized Hartree approximation based on states of form (10) and neglecting interband scattering relative simplicity has been preserved. However, if $\Omega\neq\Omega'$ then the $W_{En'}$ term will also contribute and we have breakdown of the GRPA. On calculating the eigenmodes of the system we shall see that the energies E_ν of the resonances are modified. This is the case of configuration interaction between channels Ω and Ω'. One important effect of such an interaction is to cause inelastic transitions between resonances belonging to different channels accompanied by Raman emission of a photon. It will be found that the phase shifts in this case are complex.[15] Confining ourselves to the case of 2 channels Ω and Ω' (10) takes the form

$$\Psi_E=\sum_{n\epsilon\Omega}a_{n\Omega}\phi_{n\Omega}+\sum_{n'\epsilon\Omega'}a_{n'\Omega'}\phi_{n'\Omega'}+\int dE'(b_{E'\Omega}\psi_{E'\Omega}+c_{E'\Omega'}\chi_{E'\Omega'})\tag{12}$$

and using (9)

$$\begin{aligned}(E-E_m)a_{m\Omega}&=\int dE'(b_{E'\Omega}V_{mE'}+c_{E'\Omega'}W_{mE'})\\(E-E_{m'})a_{m'\Omega'}&=\int dE'(b_{E'\Omega}W_{m'E'}+c_{E'\Omega'}V_{m'E'})\end{aligned}\tag{13}$$

and

$$\begin{aligned}Eb_{E'\Omega}&=Eb_{E'\Omega}+\sum_{n\epsilon\Omega}V_{E'n}a_{n\Omega}+\sum_{n'\epsilon\Omega'}W_{E'n'}a_{n'\Omega'}\\Ec_{E'\Omega'}&=E'c_{E'\Omega'}+\sum_{n\epsilon\Omega}W_{E'n}a_{n\Omega}+\sum_{n'\epsilon\Omega'}V_{E'n'}a_{n'\Omega'}.\end{aligned}\tag{14}$$

From (14) two orthogonal linear combinations are

$$\begin{aligned}E\{b_{E'\Omega}V_{mE'}+c_{E'\Omega'}W_{mE'}\}&=E'\{b_{E'\Omega}V_{mE'}+c_{E'\Omega'}W_{mE'}\}+\sum_{n\epsilon\Omega}(V_{mE'}V_{E'n}+W_{mE'}W_{E'n})a_{n\Omega}\\&\quad+\sum(V_{mE'}W_{E'n'}+W_{mE'}V_{E'n'})a_{n'\Omega'}\\E\{b_{E'\Omega}W_{m'E'}+c_{E'\Omega'}V_{m'E'}\}&=E'\{b_{E'\Omega}W_{m'E'}+c_{E'\Omega'}V_{m'E'}\}+\sum_{n\epsilon\Omega}(W_{m'E'}V_{E'n}+V_{m'E'}W_{E'n})a_{n\Omega}\\&\quad+\sum_{n'\epsilon\Omega'}(W_{m'E'}W_{E'n'}+V_{m'E'}V_{E'n'})a_{n'\Omega'}.\end{aligned}$$

So following Dirac[18] we may formally write

$$\begin{aligned}b_{E'\Omega}V_{mE'}+C_{E'\Omega'}W_{mE'}=&\left\{\frac{1}{E-E'}+Z_1(E')\delta(E-E')\right\}\\&\times\{\sum_{n\epsilon\Omega}(V_{mE'}V_{E'n}+W_{mE'}W_{E'n})a_{n\Omega}+\sum_{n'\epsilon\Omega'}(V_{mE'}W_{E'n'}+W_{mE'}V_{E'n'})a_{n'\Omega'}\}\end{aligned}\tag{15}$$

[18] P. A. M. Dirac, *Principles of Quantum Mechanics* (Oxford University Press, Oxford, England, 1958), 4th ed., Chap. VIII.

$$b_{E'\Omega}W_{m'E'}+C_{E'\Omega'}V_{m'E'}=\left\{\frac{1}{E-E'}+Z_2(E')\delta(E-E')\right\}$$
$$\times\{\sum_{n\epsilon\Omega}(W_{m'E'}V_{E'n}+V_{m'E'}W_{E'n})a_{n\Omega}+\sum_{n'\epsilon\Omega'}(W_{m'E'}W_{E'n'}+V_{m'E'}V_{E'n'})a_{n'\Omega'}\}. \quad (16)$$

Hence from (13),

$$(E-E_n)a_{n\Omega}=\sum(F_{mn}+G_{mn})a_{n\Omega}+Z_1(E)\sum_n(V_{nE}V_{En}+W_{nE}W_{En})a_{n\Omega}$$
$$+\sum_{n'}\{H_{mn'}+H^{\dagger}_{mn'}+Z_1(E)[V_{nE}W_{En'}+W_{mE}V_{En'}]\}a_{n'\Omega'}, \quad (17)$$

$$(E-E_{m'})a_{m'\Omega'}=\sum_{n'}(F_{m'n'}+G_{m'n'})a_{n'\Omega'}+Z_2(E)\sum_{n'}(V_{m'E}V_{En'}+W_{m'E}W_{En'})a_{n'\Omega'}$$
$$+\sum_{n}\{H_{m'n}+H^{\dagger}_{m'n}+Z_2(E)[V_{m'E}W_{En}+W_{m'E}V_{En}]\}a_{n\Omega}, \quad (18)$$

$$F_{mn}(E)\equiv P\int dE'\frac{V_{mE'}V_{E'n}}{E-E'};\quad G_{mn}(E)\equiv P\int dE'\frac{W_{mE'}W_{E'n}}{E-E'}$$
$$H_{mn}(E)\equiv P\int dE'\frac{V_{mE'}W_{E'n}}{E-E'};\quad H^{\dagger}_{mn}(E)\equiv P\int dE'\frac{W_{mE'}V_{E'n}}{E-E'}. \quad (19)$$

Equations (17) and (18) are completely symmetric in the two channels Ω and Ω' and must be solved self-consistently. We see that it is not possible to effect complete decoupling of the two channels. We may get a partial decoupling by use of perturbation theory, thereby obtaining a solution for $a_{m\Omega}$ and $a_{m'\Omega'}$. Within this approximation we shall see that it is still possible to define a collective phase shift for each channel and the eigenstates will be linear combinations of the uncoupled channels.

Firstly we diagonalize in (17) $E_m a_{m\Omega}+\sum_n(F_{mn}+G_{mn})a_n$ if the rest of the terms are small, by using

$$E_nA_{n\nu\Omega}+\sum_m(F_{mn}+G_{mn})A_{m\nu\Omega}=A_{n\nu\Omega}E_\nu \quad (20)$$

if

$$a_{n\Omega}=\sum_\nu A_{n\nu\Omega}a_{\nu\Omega};\quad \phi_{\nu\Omega}=\sum_n \phi_{n\Omega}A_{n\nu\Omega}$$

$$E\sum_\nu A_{m\nu\Omega}a_{\nu\Omega}=\sum_\nu E_\nu A_{n\nu\Omega}a_{\nu\Omega}+Z_1(E)\sum_{n,\nu}(V_{mE}V_{En}+W_{mE}W_{En})A_{n\nu\Omega}a_{\nu\Omega}$$
$$+\sum_{n'}\{H_{mn'}+H^{\dagger}_{mn'}+Z_1(E)[V_{mE}W_{En'}+W_{mE}V_{En'}]\}a_{n'\Omega'}. \quad (21)$$

For (18) we have similarly

$$a_{n'\Omega'}=\sum_{\nu'} B_{n'\nu'\Omega'}a_{\nu'\Omega'};\quad \phi_{\nu'\Omega'}=\sum_{n'}\phi_{n'\Omega'}B_{n'\nu'\Omega'}$$

$$E\sum_{\nu'}B_{m'\nu'\Omega'}a_{\nu'\Omega'}=\sum_{\nu'}E_{m'}B_{m'\nu'\Omega'}a_{\nu'\Omega'}+\sum_{n'\nu'}\{F_{m'n'}+G_{m'n'}+Z_2(E)(V_{m'E}V_{En'}+W_{m'E}W_{En'})\}B_{n'\nu'\Omega'}a_{\nu'\Omega'}$$
$$+\sum_n\{H_{m'n}+H^{\dagger}_{m'n}+Z_2(E)[V_{m'E}V_{En}+W_{m'E}V_{En}]\}a_{n\Omega}. \quad (22)$$

Now it is assumed that the resonance in the Ω' channel is far away so that

$$E_{m'}B_{m'\nu'\Omega'}+\sum_{n'}\{(F_{m'n'}+G_{m'n'})+Z_2(E)(V_{m'E}V_{En'}+W_{m'E}W_{En'})\}B_{n'\nu'\Omega'}=\mathcal{E}_{\nu'}B_{m'\nu'\Omega'}. \quad (23)$$

Using (22), (23) and the orthonormality of the A and B matrices

$$(E-\mathcal{E}_{\mu'})a_{\mu'\Omega'}=\sum_{m'}\sum_n B_{\mu'm'\Omega'}{}^{-1}\{H_{m'n}+H^{\dagger}_{m'n}+Z_2(E)[V_{m'E}W_{En}+W_{m'E}V_{En}]\}a_{n\Omega} \quad (24)$$

$$\sum_m V_{Em}A_{m\nu\Omega}\equiv V_{E\nu};\quad \sum_m W_{Em}A_{m\nu\Omega}\equiv W_{E\nu}$$
$$\sum_m V_{Em}B_{m\nu\Omega}\equiv V_{E\nu}';\quad \sum_m W_{Em}B_{m\nu\Omega}\equiv W_{E\nu}'.$$

Transforming (21) from the n to the ν representation we have

$$(E-E_\mu)a_{\mu\Omega}=Z_1(E)\sum_\nu\{V_{\mu E}V_{E\nu}+W_{\mu E}W_{E\nu}\}a_\nu+\sum_m\sum_{n'}A_{\mu m\Omega}^{-1}\{H_{mn'}+H^\dagger_{mn'}+Z_1(E)\Theta_{mn'}\}\sum_{\mu'}B_{n'\mu'\Omega'}a_{\mu'\Omega'}. \quad (25)$$

We introduce the abbreviations

$$\Theta_{mn'}\equiv V_{mE}W_{En'}+W_{mE}V_{En'};\quad \Theta_{m'n}\equiv V_{m'E}W_{En}+W_{m'E}V_{En};$$

$$\sum_{mn'}A_{\mu m}^{-1}H_{mn'}B_{n'\mu'}\equiv\Lambda_{\mu\mu'};\quad \sum_{mn'}A_{\mu m}^{-1}H^\dagger_{mn'}B_{n'\mu'}\equiv\Lambda^\dagger_{\mu\mu'};$$

$$\sum_{m'n}B_{\mu'm'}^{-1}H_{m'n}A_{n\mu}\equiv\Lambda_{\mu'\mu};\quad \sum_{m'n}B_{\mu'm'}^{-1}H^\dagger_{m'n}A_{n\mu}\equiv\Lambda^\dagger_{\mu'\mu};$$

$$\sum_{mn'}A_{\mu m}^{-1}\Theta_{mn'}B_{n'\mu'}\equiv\Theta_{\mu\mu'};\quad \sum_{m'n}B_{\mu'm'}^{-1}\Theta_{m'n}A_{n\mu}\equiv\Theta_{\mu'\mu}.$$

Then (24) and (25) and the above give,

$$(E-E_\mu)a_{\mu\Omega}=Z_1(E)\sum_\nu\{V_{\mu E}V_{E\nu}+W_{\mu E}W_{E\nu}\}a_{\nu\Omega}+\sum_{\mu'}\sum_\nu\frac{1}{(E-\mathcal{E}_{\mu'})}$$
$$\times\{\Lambda_{\mu\mu'}+\Lambda^\dagger_{\mu\mu'}+Z_1(E)\Theta_{\mu\mu'}\}\{\Lambda_{\mu'\nu}+\Lambda^\dagger_{\mu'\nu}+Z_2(E)\Theta_{\mu'\nu}\}a_{\nu\Omega}, \quad (26)$$

$$(E-E_\mu)a_{\mu\Omega}=\sum_\nu\Bigg[Z_1(E)\{V_{\mu E}V_{E\nu}+W_{\mu E}W_{E\nu}\}+\sum_{\mu'}\frac{1}{E-\mathcal{E}_{\mu'}}$$
$$\times\{\Lambda_{\mu\mu'}\Lambda_{\mu'\nu}+\Lambda_{\mu\mu'}\Lambda^\dagger_{\mu'\nu}+\Lambda^\dagger_{\mu\mu'}\Lambda_{\mu'\nu}+\Lambda^\dagger_{\mu\mu'}\Lambda^\dagger_{\mu'\nu}+Z_1(E)\Theta_{\mu\mu'}(\Lambda_{\mu'\nu}+\Lambda^\dagger_{\mu'\nu})+Z_2(E)(\Lambda_{\mu\mu'}+\Lambda^\dagger_{\mu\mu'})\Theta_{\mu'\nu}$$
$$+Z_2(E)Z_1(E)\Theta_{\mu\mu'}\Theta_{\mu'\nu}\}\Bigg]a_{\nu\Omega}. \quad (27)$$

Let us consider a transition from a resonance belonging to the Ω channel to one belonging to the Ω' channel, assuming that it is energetically favorable and dominates all other decay modes for the Ω resonance. We make the ansatz[15] that $Z_2(E)=i\pi$, in order to ensure only outgoing radiation. This assumption describes Raman decay of the Ω channel to the Ω' channel. From (27)

$$Z_1(E)i\pi\sum_{\mu'}\frac{\Theta_{\mu\mu'}\Theta_{\mu'\nu}}{E-\mathcal{E}_{\mu'}}=Z_1(E)i\pi\sum_{\mu'}\frac{\{V_{\mu E}W_{E\mu'}+W_{\mu E}V_{E\mu'}\}\{V_{\mu'E}W_{E\nu}+W_{\mu'E}V_{E\nu}\}}{(E-\mathcal{E}_{\mu'})}.$$

Also

$$i\pi\sum_{\mu'}\frac{(\Lambda_{\mu\mu'}+\Lambda^\dagger_{\mu\mu'})\Theta_{\mu'\nu}}{E-\mathcal{E}_{\mu'}}=i\pi\sum_{\mu'}\frac{1}{E-\mathcal{E}_{\mu'}}\left\{P\int dE'\frac{V_{\mu E'}W_{E'\mu'}}{E-E'}+P\int dE'\frac{W_{\mu E'}V_{E'\mu'}}{E-E'}\right\}\{V_{\mu'E}W_{E\nu}+W_{\mu'E}V_{E\nu}\}.$$

Clearly, near the resonance in the Ω channel and far from the resonance in Ω' channel $\mathcal{E}_{\mu'}\simeq E_{\mu'}$

$$\sum_{\mu'}\frac{\Theta_{\mu\mu'}\Theta_{\mu'\nu}}{E-E_{\mu'}}\gg\sum_{\mu'}\frac{(\Lambda_{\mu\mu'}+\Lambda^\dagger_{\mu\mu'})\Theta_{\mu'\nu}}{E-E_{\mu'}}. \quad (28)$$

Again the extra real terms in (27) are small if $W\ll V$ and contribute to a real energy shift. This energy shift, however, changes the position of the Ω channel resonances and this is due to the configuration interaction between the two channels. Assume that this energy shift is small then

$$(E-E_\mu)a_{\mu\Omega}\simeq Z_1(E)\sum_\nu\{V_{\mu E}V_{E\nu}+i\pi\sum_{\mu'}(\Theta_{\mu\mu'}\Theta_{\mu'\nu}/(E-E_{\mu'}))\}a_{\nu\Omega}. \quad (29)$$

Equation (29) is of the form (85) of Van Kampen,[15] while $a_\mu=\sum_\nu T_{\mu\nu}a_\nu$, from which the secular equation determines the phase shift $Z_1(E)$. Applying (29) to a case of two channels, with one resonance per channel, we get that

$$-\frac{\tan\Delta_\Omega(E)}{\pi}=\frac{1}{Z_1(E)}=\frac{|V_{E1}|^2}{E-E_1}+i\pi\frac{|\Theta_{11'}|^2}{(E-E_1')(E-E_1)}.$$

In general then, we may write

$$\tan\Delta_\Omega(E)=-\frac{\pi}{Z_1(E)}=-\pi\sum_\nu\left\{\frac{|V_{E\nu}|^2}{E-E_\nu}+i\pi\sum_{\nu'}\frac{|\Theta_{\nu\nu'}|^2}{(E-E_\nu)(E-E_{\nu'})}\right\}. \quad (30)$$

Again following Van Kampen and generalizing the collective phase shift for channel Ω (30) assumes the form.

$$\tan\Delta_\Omega(E)=-\pi\sum_\nu\left\{\frac{|V_{E\nu}|^2}{\omega_\nu}+i\pi\sum_{\nu'}\frac{|\Theta_{\nu\nu'}|^2}{\omega_\nu\omega_{\nu'}}\right\} \quad (31)$$

$$\omega_\nu\equiv E-E_\nu+i\pi\sum_{\nu'}\Theta_{\nu\nu'}.$$

It is seen that the system of equations have a simple meaning only if the energy is near that of a resonance in any channel. Then, partial decoupling of the channels is simple and the collective phase shift for that channel is defined. If we consider the region directly in between two resonances of equal strength belonging to different channels then it is not possible to separate collective phase shifts belonging to separate channels. This is the case of strongly overlapping resonances. Again a simple form (31) cannot be obtained unless it is assumed that $V\gg W$ so that in this weak-coupling case the interband scattering is much less than the intraband scattering. Hence the effect of the photon decay from channel Ω to channel Ω' is to cause an imaginary term to be added to the collective phase shift of Ω.

To calculate the dielectric response of the system we can consider two special cases: (1) completely independent channels, and (2) when these are mixed by inelastic scattering.

For completely independent channels Ω and Ω',

$$\Psi_{1E}=\sum a_{n\Omega}\phi_{n\Omega}+\int dE' b_{E'\Omega}\psi_{E'},$$

$$\Psi_{2E}=\sum a_{n'\Omega'}\phi_{n'\Omega'}+\int dE' c_{E'\Omega'}\chi_{E'}, \quad (32)$$

$$|\langle\Psi_E|T|i\rangle|^2=|\langle\Psi_{1E}|T|i\rangle|^2+|\langle\Psi_{2E}|T|i\rangle|^2.$$

And analogous to (11)

$$\epsilon_2(E)=\sum_\Omega\cos^2\Delta_\Omega(E)\,|\sum_{\nu\epsilon\Omega}q_\nu\tan\Delta_{\nu\Omega}(E)-1|^2\epsilon_\Omega(E), \quad (33)$$

where the collective phase shifts Δ_Ω, $\Delta_{\Omega'}$ of the two channels are wholly real and $\epsilon_\Omega(E)$, $\epsilon_{\Omega'}(E)$ represent the contribution from the scattering states belonging to channels Ω and Ω', respectively. It is noticed that the antiresonances generated in channel Ω may be destroyed by the contribution to $\epsilon_2(E)$ coming from the second term of (33) and similarly for Ω' antiresonances.[19,20] This term will be particularly effective if $\epsilon_{\Omega'}(E)$ is large. The effect is due to the lack of coherence between the two channels. This then corresponds to GRPA.

For the case when the channels Ω and Ω' are mixed by inelastic scattering we must choose linear combinations of eigenfunctions belonging to independent channels and find the new eigenstates ψ_{n+}, ψ_{n-} of the system in which the channels are coupled only through an imaginary term in the phase shift. The response is given by (32), where

$$\Psi_{1E}=\sum_{n\epsilon\Omega}a_{n\Omega}\phi_{n\Omega}+\sum_{n\epsilon\Omega}\int dE'(b_{E'\Omega}V_{nE'}+c_{E'\Omega'}W_{nE'})\psi_{n+}(E'),$$

$$\Psi_{2E}=\sum_{n'\epsilon\Omega'}a_{n'\Omega'}\phi_{n'\Omega'}+\sum_{n\epsilon\Omega}\int dE'(-b_{E'\Omega}W_{nE'}+c_{E'\Omega'}V_{nE'})\psi_{n-}(E'), \quad (34)$$

ψ_{n+} and ψ_{n-} are symmetric and antisymmetric linear combinations of the independent-channels' degenerate scattering eigenstates. From (13) it is seen that ψ_{n+} is to be used for Ω channel if it is assumed that the energy is near one of the resonances belonging to it, while ψ_{n-} is used near a resonance in the Ω' channel.

It is very easily seen that

$$\psi_{n+}(E)=\frac{V_{nE}\psi_E+W_{nE}\chi_E}{(|V_{nE}|^2+|W_{nE}|^2)^{1/2}},$$

$$\psi_{n-}(E)=\frac{-W_{nE}\psi_E+V_{nE}\chi_E}{(|V_{nE}|^2+|W_{nE}|^2)^{1/2}}. \quad (35)$$

Corresponding to (33) we get now for complex phase shifts $\bar\Delta_\Omega$, $\bar\Delta_{\Omega'}$

$$\epsilon_2(E)=(1+|\tan\bar\Delta_\Omega(E)|^2)^{-1}|\sum_{\nu\epsilon\Omega}\bar q_\nu\tan\bar\Delta_{\nu\Omega}(E)-1|^2\bar\epsilon_\Omega(E)+(1+|\tan\bar\Delta_{\Omega'}(E)|^2)^{-1}\times|\sum_{\nu'\epsilon\Omega'}\bar q_{\nu'}\tan\bar\Delta_{\nu'\Omega'}(E)-1|^2\bar\epsilon_{\Omega'}(E), \quad (36)$$

where

$$\bar\epsilon_\Omega(E)=\sum|\langle\psi_{n+}|T|i\rangle|^2;\quad \bar\epsilon_{\Omega'}(E)=\sum|\langle\psi_{n-}|T|i\rangle|^2,$$

$\bar q_\nu$, $\bar q_{\nu'}$ are oscillator strengths measured relative to the scattering states ψ_{n+} and ψ_{n-}, respectively. It is seen that (36) is formally similar to (33) with some differences. Firstly the phase shifts $\bar\Delta_\Omega$, $\bar\Delta_{\Omega'}$ are complex. Secondly, by a suitable choice of the variables in (35) $\psi_{n-}(E)$ may be made to vanish, so that the noncoherence of the scattering states $\psi_{n+}(E)$, $\psi_{n-}(E)$ does not destroy completely the antiresonances of the peaks in question. It will be seen that the line shapes for the

[19] This result is consistent with Wigner's general theorem that elastic cross sections do not vanish (i.e., exhibit perfect antiresonances) for any value of the energy except in one-channel reactions. With regard to Raman decay he also shows that the reaction cross section vanishes for discrete values of the energy in 2-channel reactions. In three or more channel reactions no reaction cross section vanishes in general for any value of the energy. See Ref. 20.

[20] E. P. Wigner, Proc. Natl. Acad. Sci. U. S. 32, 302 (1946).

mixed channel case are significantly different from those of the single-channel or independent-channels case.

4. GENERATION OF LINE SHAPES

Using the ideas of the preceding sections it is now possible to analyze theoretically the optical absorption line shapes above the fundamental absorption edge. For detailed analysis we have focussed our attention on the solid rare gases, whose spectra are simplified by the absence of optical phonons and correspondingly weak polaron effects.[21] Recently, Baldini[16] has carried out measurements of the ultraviolet absorption spectra of solid rare gases both for annealed and unannealed samples. In particular we analyze in detail the spectra of solid xenon. The resonant structure has been identified and interpreted in terms of the solid-xenon band structure.[5] (See Fig. 2.)

So far the proper self-energies of the coherent exciton-photon field have been considered, but no mention has been made of the exciton-exciton interactions mediated by the incoherent phonon field. In addition to the width $\Gamma_\nu=2\pi V_E^2$ corresponding to the coherent exciton-photon field, we also introduce a width γ_ν corresponding to the damping of exciton resonances induced by the incoherent exciton-phonon field. The incoherent width γ_ν is taken into account by folding expressions for the dielectric response with a Gaussian of width γ_ν

$$\epsilon_2(E)=\frac{1}{\sqrt{2\pi}}\int_{-\infty}^{\infty}dE'\frac{\epsilon_2(E')}{\sigma}\exp\left[-\left(\frac{E-E'}{\sigma}\right)^2\right] \quad (37)$$

where $\sigma=\frac{1}{2}\gamma$. The ratio γ_ν/Γ_ν determines the depth of the antiresonance below the background density of states. It is found that starting from $\gamma_\nu=0$, a situation of perfect antiresonance, as γ_ν increases the antiresonance becomes progressively shallower. Again if q_ν, the line shift and the width function Γ_ν are assumed to be nearly energy-independent then

$$\int dE[|\langle\Psi_E|T|i\rangle|^2-|\langle\psi_E|T|i\rangle|^2]=|\langle\psi_E|T|i\rangle|^2\frac{\pi}{2}\Gamma_\nu(q_\nu^2-1). \quad (38)$$

Therefore the excess transition probability due to the resonant state over the scattering states determines the parameter q_ν. In actual analysis the parameter q_ν which is a measure of the total amplitude strength of that resonance, is determined by planimetry of the experimental line shape. The sign of q is taken to be negative corresponding to attractive electron-hole interaction so that the antiresonance falls on the high-energy side of the resonance. The widths γ_ν, Γ_ν are phenomenological parameters which are varied in order to fit the experiment. The resonant energies E_ν are taken from the experiment also.

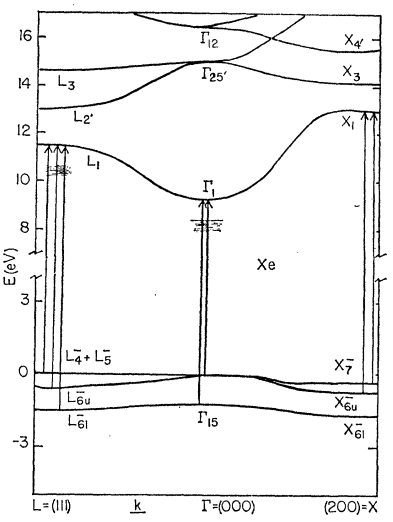

FIG. 2. The energy bands of solid xenon (after Phillips, Ref. 5). The regions whence the wave packets for the Γ and L excitons are mainly taken are indicated by the shading.

Because of the strongly overlapping resonances, and in some cases of composite structures, it is convenient to interpolate the phonon Gaussian parameter as a continuous function of energy

$$\gamma_{\text{eff}}^2(E)=\sum_\nu\frac{\gamma_\nu^2}{(E-E_\nu)^2}\Big/\sum_\nu\frac{1}{(E-E_\nu)^2}. \quad (39)$$

Near each individual resonance $\gamma_{\text{eff}(E)}\to\gamma_\nu$ and provides the ratio γ_ν/Γ_ν for that resonance.

It is not possible, *a priori*, to separate the absorption due to the resonant structure from that due to the continuum states directly from the experimental curve. Yet it is possible to make an "educated guess" as to its form. The energy bands of xenon (Fig. 2) have been inferred[5] from experiment by analogy with Mattheiss'[22] calculation of the band structure of solid argon. This then gives for the background density of states of xenon a square root behavior at absorption edge and a saddle-point singularity at the edge of the zone. Also due to the long range effect of the Coulomb interaction on scattering states the absorption coefficient at the absorption edge goes to a constant rather than zero.[12]

Using Elliott's notation[12] the absorption coefficient μ is given by

$$\mu=(2\pi/vc)\sum_n|\langle 0|\sigma|0,n\rangle|^2S_n(E),$$

where $S_n(E)$ is the density of states per unit energy range. Introducing

$$f_n=(2n/he^2\nu)|\langle 0|\sigma|0,n\rangle|^2,$$

$$\mu=(\pi e^2h/mc)\sum_n f_nS_n(E),$$

since

$$S_n(E)=G^{1/2}/2BE^{3/2}=(n/2BE),$$

$$\mu=(\pi e^2h/2mcB)\sum(nf_n/E_n). \quad (40)$$

[21] H. Frohlich, H. Pelzer, and S. Zieman, Phil. Mag. **41**, 221 (1950).

[22] L. F. Mattheiss, Phys. Rev. **133**, A1399 (1964).

Hence, the absorption coefficient can be determined from (40) if the total oscillator strength below the direct absorption threshold is known. Other features, such as absorption by surface or volume impurities, may influence the choice of background. In actual practice a number of phenomenological background density of states must be tried.

In general, optical experiments are carried out by measuring either the reflectance[23] or the absorption[16] of the incident beam. In the former case the real and imaginary parts of the dielectric response are gotten from the data by the use of Kramers-Kronig transforms. In the latter case the optical density $\mu d/2.303$ is measured, where d is the thickness of the film and μ the absorption coefficient. To make contact with the absorption experiment, $\epsilon_1(E)$ is calculated from the theoretical expression for $\epsilon_2(E)$ by the use of Kramers-Kronig[24] transforms

$$\epsilon_1(E)=\epsilon_1(\infty)+\frac{2}{\pi}P\int_0^\infty dE'\frac{\epsilon_2(E')E'}{E'^2-E^2}. \tag{41}$$

From $\epsilon_1+i\epsilon_2=(n+ik)^2$ and $\mu=4\pi k/\lambda$ where n and k are the optical constants, the absorption coefficient μ can be determined:

$$\mu(E)=\frac{\sqrt{2}E}{\hbar c}\{-\epsilon_1(E)+(\epsilon_1^2(E)+\epsilon_2^2(E))^{1/2}\}^{1/2}. \tag{42}$$

The line shapes generated by (42) can then be directly compared with the experiment, providing that the effects of spatial dispersion[25] can be neglected. It is seen from (41) that $\epsilon_2(E)$ must be known over the entire energy range in order to calculate $\epsilon_1(E)$. This point will be further discussed in Sec. 5.

5. ANALYSIS OF THE SOLID-XENON ULTRAVIOLET ABSORPTION SPECTRA

The results of the previous sections are now applied to the numerical analysis of the solid-xenon ultraviolet spectra and compared with Baldini's[16] measurements. Solid xenon has a fairly rich resonant optical structure particularly for annealed specimens below 20°K. For the unannealed sample the structure is strongly broadened by the scattering from lattice defects. Following Phillips[5] we note that in addition to the 2 families of hydrogenic excitons, the $\Gamma(\frac{3}{2})$ and $\Gamma(\frac{1}{2})$, there also exist metastable saddle-point excitons, $L(\frac{3}{2})$ and $L(\frac{1}{2})$. The letters refer to the symmetry of the parent interband edges and the $\frac{3}{2}, \frac{1}{2}$ refer to the J value of the spin-orbit split valence band.

Let us now construct a background density-of-states curve. For solid xenon the direct absorption threshold for the $\Gamma(\frac{3}{2})$ band is at 9.28 eV. The position of the $\Gamma(\frac{1}{2})$ threshold is not observed but can be inferred as follows. The binding energy of the $1s\,\Gamma(\frac{3}{2})$ exciton is 0.92 eV. If there were no interaction between the $\Gamma(\frac{1}{2})$ and L excitons, the limit of the $\Gamma(\frac{1}{2})$ series would be 1.22 eV above that of the $\Gamma(\frac{3}{2})$ excitons, i.e., by the spin-orbit splitting of the valence bands at Γ_{15}. Consequently the onset of the $\Gamma(\frac{1}{2})$ threshold occurs at 10.50 eV and falls between the $L(\frac{3}{2})$ and $L(\frac{1}{2})$ excitons. Below the absorption edge a constant absorption background was assumed due to volume and surface defects. This was then joined smoothly with the scattering states above the threshold.

To separate the background into two channels we assume that both for the $\Gamma(\frac{3}{2})$ and $\Gamma(\frac{1}{2})$ channels the background curves are additive and of the same form. Then the total background $B(E)$ must be obtained from a difference equation:

$$B(E)=H(E)+H(E-3\lambda/2), \quad E>3\lambda/2.$$

Here $H(x)$ is the joint background density of states curve for the $\Gamma(\frac{3}{2})$ channel and $3\lambda/2$ is the spin-orbit splitting of the valence bands at the point Γ_{15}. The scattering states curve for the two pairs of bands, which constitute the channels Ω and Ω' is indicated in Fig. 3.

In the present example (41) gives

$$\epsilon_1(E)=1+\frac{2}{\pi}P\int_0^\infty dE'\frac{\epsilon_2(E')E'}{E'^2-E^2}. \tag{41'}$$

It is seen that $\epsilon_2(E)$ must be known over the entire energy range in order to calculate the above integral. Baldini's data goes up only to 13.8 eV. Near this energy it is noticed that there is considerable contribution to the absorption from the X edge which must be included. For the Γ and L regions the shape of $\epsilon_2(E)$ is similar in xenon to that of the alkali halides, and also the band structures are similar. Hence from 13.8 to 25 eV use is made of the KBr reflectance data of Philipp and

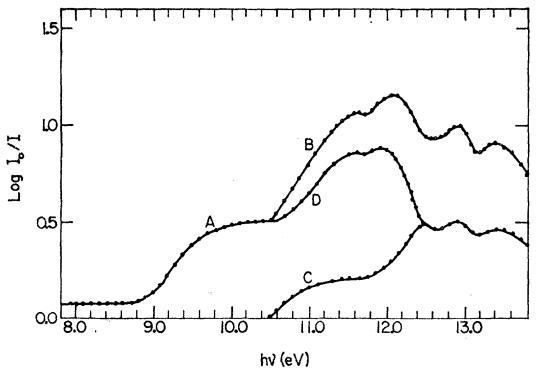

FIG. 3. The background density of states for solid xenon. The curve AD gives the contribution to the channel containing the $\frac{3}{2}$ resonances; C gives that to the $\frac{1}{2}$ resonances. The total background density of states is given by AB. Above 12.25 eV separation into the two channels is redundant.

[23] H. R. Phillip and E. A. Taft, Phys. Rev. **133**, 1002 (1959).
[24] C. Kittel, *Elementary Statistical Physics* (John Wiley & Sons, Inc., New York, 1958).
[25] S. I. Pekar, Zh. Eksperim. i Teor. Fiz. **33**, 1022 (1957) [English transl.: Soviet Phys.—JETP **6**, 785 (1958)].

TABLE I. Phenomenological parameters necessary for the optimum fit to the annealed spectrum of Baldini (Ref. 16).

	$\Gamma(\frac{3}{2})$				$\Gamma(\frac{1}{2})$			$L(\frac{3}{2})$		$L(\frac{1}{2})$
	$1s$	$2s$	$3s$	lim	$1s$	$2s$	lim			
E (eV)	8.36	9.08	9.20	9.28	9.53	9.75	9.90	10.21	10.42	11.16
γ_ν (eV)	0.14	0.06	0.04	0.02	0.32	0.18	0.2	0.34	0.34	0.54
Γ_ν (eV)	0.014	0.006	0.004	0.002	0.032	0.018	0.028	0.034	0.048	0.054
$-q_\nu$	10.81	4.34	1.08	1.01	4.07	2.43	2.40	2.77	2.34	3.31

Ehrenreich[26] to determine the shape of $\epsilon_2(E)$. The magnitude can be determined by scaling appropriately by the ratio of the static dielectric constants[27]

$$\epsilon_0(\mathrm{Xe})/\epsilon_0(\mathrm{KBr})=2.23/2.43=0.918.$$

Above 25 eV an E^{-4} form is assumed for $\epsilon_2(E)$, but it makes little difference in our results for the region below 14 eV.

The resonant energies E_ν, the approximate oscillator amplitudes q_ν and widths (of the strongly overlapping resonances) are obtained by fitting Baldini's measurements. The $L(\frac{3}{2})$ exciton peak is assumed to be composite,[5] the two associated peaks being unresolved due to their phonon widths. The line shapes in various theoretical approximations (see below) were generated on the IBM 7094 at the Computation Center of the University of Chicago. Extensive use was made of the cathode-ray tube (CRT) facilities there, which provided the plotted line shapes on photographic film.

(A) Annealed Spectrum

(1). *Single-Channel Approximation*

It is assumed that there is only one continuum of scattering states AB (see Fig. 3) and that all resonances autoionize into it. Values of the widths Γ_ν are chosen phenomenologically and those of γ_ν are chosen as indicated by the experiment. Then using (11), (37), (38), (39), (41′), and (42) the absorption line shapes are generated by varying the ratio γ_ν/Γ_ν. Also since it is not possible, for strongly overlapping resonances, to determine precisely the oscillator amplitudes of the individual resonances, the q_ν's are also varied a little from values initially estimated graphically to get better agreement with experiment.

Now since the above calculations can only really represent the upper bound of Γ_ν, the ratio γ_ν/Γ_ν is minimized for each resonance by increasing Γ_ν until the theoretical line shapes are quite different from the experimental ones. In this manner the Γ_ν's of the resonances were maximized. Various values of Γ_ν, γ_ν, E_ν are given in Table I [the γ_ν and Γ_ν of $L(\frac{1}{2})$ exciton were 0.66 and 0.066 eV, respectively]. It is seen that the minimum value of γ/Γ was between 7 and 10 for all the resonances. The peak at $L(\frac{3}{2})$ is composite and the resonant energies of the two basic peaks which go to make up this composite structure are varied a little until the line shape is similar to the experimental one. The optimum fit is shown in Fig. 4.

The most sensitive part of the analysis rests in obtaining the correct depth and shape for the antiresonances at 10.05, 10.65, and 11.28 eV. In the single channel approximation we see that the V-shaped antiresonances at 10.05 and 10.65 eV are too shallow. Further deepening by decrease of γ_ν/Γ_ν results in a poor over-all line shape. Also the antiresonance at 11.28 eV is much too deep. It is possible to make it shallower by increasing γ_ν/Γ_ν at a constant γ_ν by decreasing Γ_ν. A reasonable fit for $L(\frac{1}{2})$ is obtained for unrealistic values of γ_ν/Γ_ν ($\sim$30) but the remaining structure does not fit so well. Alternatively the $L(\frac{1}{2})$ antiresonance may be filled in by increasing the γ_ν belonging to it. In this case again unrealistic values of γ_ν are required ($\sim$1.0 eV) and further the antiresonance at 10.65 eV becomes even shallower. Hence we feel that Fig. 4 does represent the optimum fit, the deviations of the calculated line shape from the experimental one being due to the inadequacy of the single channel approximation.

(2). *Two-Channel Approximation*

(i) *Independent channels* Ω *and* Ω'. Here use is made of (33) instead of (11) for generating the line shapes. The functions $\epsilon_\Omega(E)$ and $\epsilon_{\Omega'}(E)$ used for the two chan-

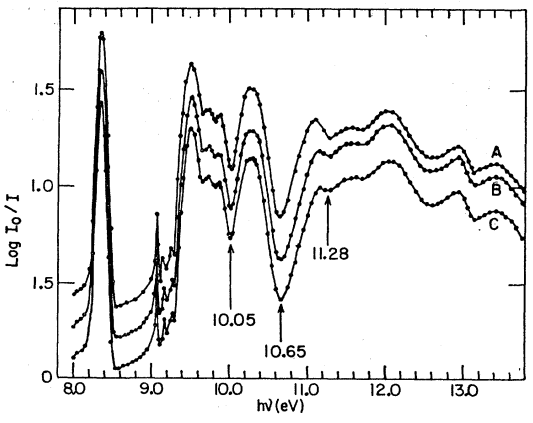

FIG. 4. Theoretical line shapes for annealed solid xenon. A represents the optimum fit for the single-channel approximation; C that for two independent channels; B that for two mixed channels. The ordinates for A, B, and C are staggered by 0.16.

[26] H. R. Philipp and H. Ehrenreich, Phys. Rev. 131, 2016 (1963).
[27] Only the electronic polarizabilities contribute to ϵ_0. In literature this is frequently designated by $\epsilon(\infty)$.

nels correspond to C and AD, respectively, in Fig. 3. The resonances $L(\frac{1}{2})$ and $\Gamma(\frac{1}{2})$ belong to the Ω channel while $L(\frac{3}{2})$ and $\Gamma(\frac{3}{2})$ belong to Ω'. It is noticed in Fig. 4, as expected, that the antiresonance at $L(\frac{1}{2})$ is nearly quenched due to the incoherent contribution to $\epsilon_2(E)$ coming from the scattering states of the Ω' channel. Also the antiresonance at 10.65 eV is too deep. The collective phase shifts of the channels Ω and Ω' are wholly real.

(ii) *Mixed channels.* Here use is made of (36) and its subsidiary equations instead of (11) for generating the line shapes, the phase shifts now being complex. The expression (31) is greatly simplified if it is assumed that Raman decay occurs only into the nearest excitons of the other channel. The effect of decay to other excitons is negligible due to the large energy denominators for excitons widely separated in energy. Excitons belonging to the same channel cannot Raman decay directly into each other since the Hamiltonian is already diagonal in that part which would induce such transitions. Again resonances decay into ones which are at a lower energy.

The optimum parameters as determined from the single-channel approximation are carried over and various values of the interband scattering parameter W are tried. The procedure adopted is as follows: (i) Assign W/V; (ii) line shapes generated for various values of W and V keeping the ratio a constant; (iii) the V's are maximized; (iv) processes (i) and (iii) repeated until self-consistency is attained. The width and the depth of the antiresonances depends strongly on the ratio W/V, since this determines both the collective phase shift Δ, ψ_{n+} and ψ_{n-}. Figures 5 and 6 show the line shapes for $W/V=0.1$, 0.2, and 0.3. We feel that the optimum fit is obtained for $W/V=0.1\pm0.03$. For this ratio the antiresonances at 10.05 and 10.65 eV are deepened from their single-channel values and the one at 11.28 eV made shallower so that sound agreement is obtained with the experiment. The theoretical line shape is a very sensitive function of the interband scattering to autoionization ratio W/V as is shown in Fig. 5. On increasing W/V from 0.1 to 0.2 we see that the antiresonance at 10.65 becomes less shallow and that at 11.28 too deep. This effect becomes even more pronounced as W/V becomes 0.3. Table I gives the parameters for the optimum fit in the mixed channel approximation. In order to illustrate the extension of $\epsilon_2(E)$ up to 25 eV for the Kramers-Kronig integral, the dielectric function for the optimum fit is given in Fig. 7.

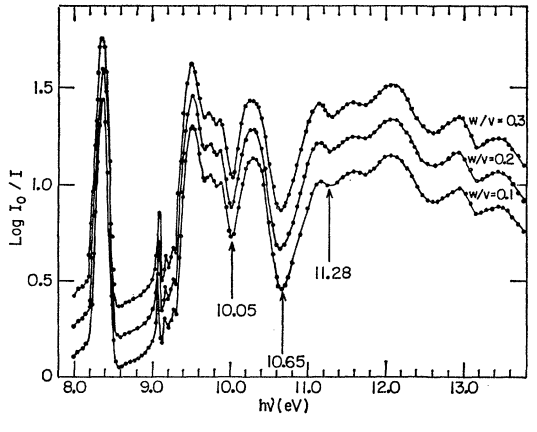

FIG. 5. Theoretical line shapes for annealed solid xenon for the mixed two channels approximation. Values of W/V used are 0.1, 0.2, and 0.3. The ordinates for the various line shapes are staggered by 0.16.

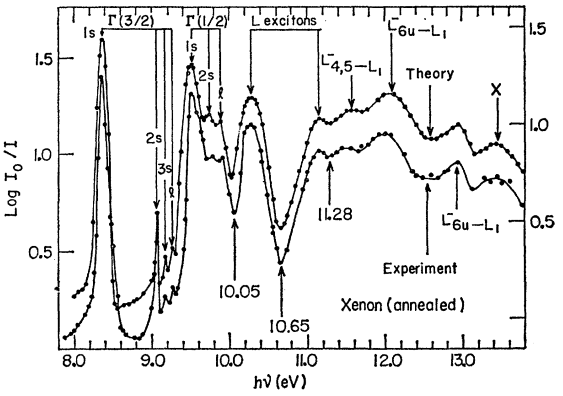

FIG. 6. Comparison of the best theoretical line shape of xenon corresponding to $W/V=0.1$ with that of the annealed one of Baldini. Antiresonances at 10.05, 10.65, and 11.28 eV are very important. The ordinates are staggered by 0.16.

We have used the approximation that q, V, W belonging to various resonances are energy-independent. In actual fact these parameters depend upon the background density of states which is energy-dependent. If the energy dependence of these parameters is considered then q_ν is no longer simply related to the oscillator amplitude of the peak. For example according to Fano

$$q_\nu=\frac{\langle\bar{\Phi}_\nu|T|i\rangle}{\pi V_{E\nu}\langle\psi_E|T|i\rangle};\quad \bar{\Phi}_\nu=\bar{\phi}_\nu+P\int dE'\frac{\psi_{E'}V_{E'\nu}}{E-E'}.$$

The energy dependence of q_ν, $V_{\nu E}$ and $W_{\nu E}$ is very complex. Accordingly in the above numerical analysis we have neglected the energy dependence of these parameters.

(B) Discussion

The experimental absorption line shape of solid xenon contains two striking antiresonances in the form of symmetrical V's at 10.05 and 10.65 eV. In addition there is a very shallow antiresonance at 11.28 eV. It is our contention that any theoretical model for the line shapes must account not only for the peak strengths and widths but also for these antiresonances which give rise to the asymmetries of the resonances. It seems unlikely that line shapes generated by superposition of simple Lorentzians would exhibit such asymmetries. However, the theoretical line shapes calculated on the basis of the coherent exciton-photon field, with the phenomeno-

logical parameters γ_ν and Γ_ν, are in good agreement with the experimentally observed ones. Hence we feel that the interference effects associated with the exciton-photon interaction, instead of the exciton-phonon interaction, must be the basic mechanism responsible for the observed absorption line shapes. Within the single-channel approximation the depths of the antiresonances deviate from experiment. Breakdown of the GRPA has to be invoked in order to adjust correctly the depths of the antiresonances. Here, as has been mentioned, Wigner's[20] general theorem plays a fundamental role.

One of the by-products of our analysis of solid xenon is the fact that we confirm the conjecture[5] that the $L(\frac{3}{2})$ exciton is a composite peak of two excitons. These are separated in energy by 0.21 ± 0.03 eV. They arise from the parent edges $L_{4,5}^- \rightarrow L_1$ and $L_{6u}^- \rightarrow L_1$ which are separated in energy by 0.5 eV. This can be explained on the basis of configuration interaction as done in Sec. 6.

Another by-product of our analysis is that it enables us to estimate the relative magnitude of the interband to the intraband scattering matrix elements. The autoionization parameter $V_{E\nu}^2=C^2N_\Omega(E_\nu)$, whilst the inelastic decay parameter $W_{E\nu}^2=(C')^2N_{\Omega'}(E_\nu)$. The $N_\Omega(E_\nu)$ and $N_{\Omega'}(E_\nu)$ are the background density of states of the channels Ω and Ω' at E_ν, C and C' are the intraband and interband scattering matrix elements, respectively:

$$\frac{C}{C'}=\frac{V_{E\nu}}{W_{E\nu}}\left(\frac{N_{\Omega'}(E_\nu)}{N_\Omega(E_\nu)}\right)^{1/2}. \tag{43}$$

For $L(\frac{1}{2})$ exciton in solid xenon, $[N_{\Omega'}(E_\nu)/N_\Omega(E_\nu)]^{1/2}\sim2.10$, $V_{E\nu}/W_{E\nu}\sim10\pm3$, so that $C/C'\sim21\pm6$.

It may be argued that there may also be phonon-induced photon emission due to interactions among resonances belonging to the same channel. This is a very difficult field-theoretical problem and according to our knowledge has, as yet, not been investigated.

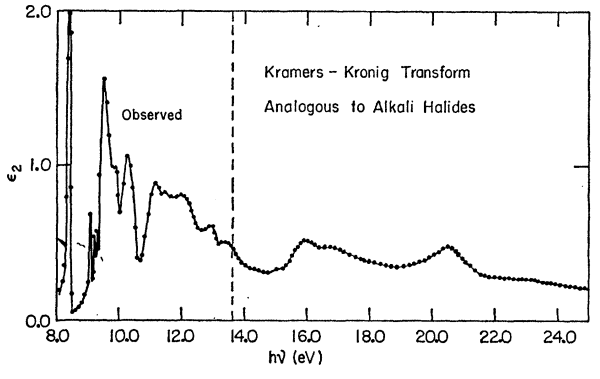

FIG. 7. Theoretical $\epsilon_2(E)$ for the optimum mixed 2 channels showing extension up to 25 eV using the data of Ehrenreich and Philipp for KBr (Ref. 26). This is necessary in order to carry out the Kramers-Kronig integrals to obtain the absorption coefficient.

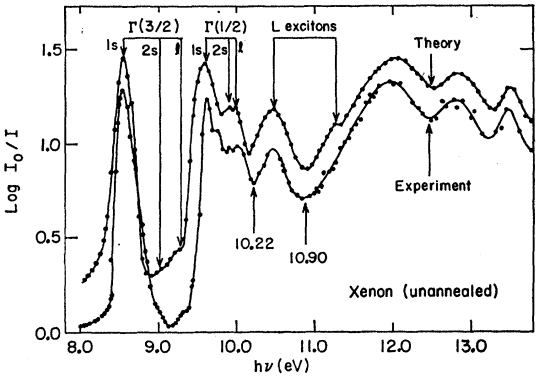

FIG. 8. Comparison of the best theoretical line shape of xenon corresponding to $W/V=0.0$ with that of the unannealed one of Baldini. Note that the calculated antiresonances are not sufficiently broadened. The ordinates are staggered by 0.16.

(C) Unannealed Spectrum

It is seen in Fig. 8 that the peaks are much broadened due to scattering from phonons and lattice defects. The resonant energies in the unannealed spectrum have shifted towards higher energies in comparison to those of the annealed case. The only exception to this is the series limit of the $\Gamma(\frac{3}{2})$ series. One of the factors that probably contributes to this is that in the unannealed sample the crystal structure is not completely fcc but rather it is mixed in with hcp. Phillips[5] has suggested that for excitons of small radius this difference in the crystal structure from that of the annealed sample (completely fcc) quenches the anisotropic contribution to exciton binding energies. Excitons near the series limit have large radii so that for these the crystal structure is no longer significant. Hence the limit of the $\Gamma(\frac{3}{2})$ series remains the same.

The $L(\frac{1}{2})$ exciton seems to be nearly quenched in the experimental data of Baldini; in fact it is hard to discern any peak at all. For our theoretical analysis we have shifted the $L(\frac{1}{2})$ peak by 0.14 eV from its value in the annealed sample.

In generating the line shapes theoretically we have assumed that the lattice scattering is much larger in the unannealed than in the annealed sample so that the peaks are very broad. The resonant energies are taken from experiment and the line shapes were generated in the two channel approximation. It is seen in Fig. 8 that a broad, shallow antiresonance is obtained at 10.9 eV. The $L(\frac{1}{2})$ resonance at 11.40 eV, though very weak, is not completely quenched. The experimental data in this region show considerable scatter, which may or may not indicate the presence of fine structure similar to our weak antiresonance. The deviation, below the threshold, of the calculated line shapes from those observed experimentally may again be attributed to the absorption on the surface of the film or to other defect-induced spatial inhomogeneities (see Appendix). The parameters used in generating Fig. 8 are given in Table II.

TABLE II. Phenomenological parameters necessary for the optimum fit to the unannealed spectrum of Baldini (Ref. 16).

	$\Gamma(\frac{3}{2})$			$\Gamma(\frac{1}{2})$			$L(\frac{3}{2})$		$L(\frac{1}{2})$
	$1s$	$2s$	lim	$1s$	$2s$	lim			
E (eV)	8.56	9.03	9.28	9.62	9.90	10.02	10.37	10.58	11.30
γ_ν (eV)	0.32	0.28	0.02	0.56	0.170	0.160	0.62	0.60	0.70
Γ_ν (eV)	0.032	0.028	0.002	0.056	0.017	0.016	0.062	0.06	0.07
$-q_\nu$	10.32	1.52	1.40	3.90	1.80	1.83	2.30	2.32	4.03

Our treatment of the spectrum has assumed spatial homogeneity (translational invariance) of the sample, i.e., the scattering and resonance states are constructed by taking configuration averages. By comparing our theoretical line shape in Fig. 8 with the experimental spectrum we are led to suspect that this assumption is not entirely valid for the unannealed sample. In particular, the antiresonances preceding and following the $L(\frac{3}{2})$ resonance at 10.9 eV are too narrow. More evidence for localization is provided by the high-energy satellite of the $\Gamma(\frac{1}{2})$ $1s$ resonance. This satellite is not present in the annealed spectrum; it appears to be associated with $\Gamma(\frac{1}{2})$ $1s$ resonances localized near defects (e.g., stacking faults).

6. CONFIGURATION INTERACTION IN XENON

Initially the energies of the resonant states E_n in Eq. (9) do not contain any contribution due to the admixture of either the scattering states or other exciton states. These energies are shifted by configuration interaction in two ways. Firstly there is the effect of interaction both with the scattering states and resonant states belonging to the parent channel. Secondly there is the effect of interaction with states belonging to a different channel (corresponding to the breakdown of the GRPA).

(i). Consider first the energy shifts within the GRPA so that in Eq. (20) G_{mn} is zero. The secular equation determining the resonant energies is gotten from

$$E_n A_{n\nu\Omega}+\sum_m F_{mn}A_{m\nu\Omega}=A_{n\nu\Omega}E_\nu, \tag{44}$$

where $F_{mn}(E)$ is given by (19) and is a matrix representing second-order interaction among the resonances arising from their coupling with the intermediate scattering states. Hence E_ν represents the new resonant energies, its difference from E_n being due to the real part of the proper self-energies of the exciton photon field. Similarly resonances belonging to another scattering channel Ω' have resonant energies denoted by $E_{\nu'}$. In fact the entire energy matrix for two channels Ω and Ω' containing n and n' resonances, respectively, is

$$\begin{pmatrix} \begin{pmatrix} E_1-\lambda+F_{11} & F_{12} & \cdots & F_{1n} \\ \vdots & & & \vdots \\ F_{n1} & \cdots & F_{nn-1} & E_n-\lambda+F_{nn} \end{pmatrix} & \begin{pmatrix} \Lambda_{11'} & \Lambda_{12'} & \cdots & \Lambda_{1n'} \\ \vdots & & & \vdots \\ \Lambda_{n1'} & \Lambda_{n2'} & \cdots & \Lambda_{nn'} \end{pmatrix} \\ \begin{pmatrix} \Lambda_{1'1} & \Lambda_{1'2} & \cdots & \Lambda_{1'n} \\ \vdots & & & \vdots \\ \Lambda_{n'1} & \Lambda_{n'2} & \cdots & \Lambda_{n'n} \end{pmatrix} & \begin{pmatrix} E_{1'}-\lambda'+F_{1'1'} & F_{1'2'} & \cdots & F_{1'n'} \\ \vdots & & & \vdots \\ F_{n'1'} & \cdots & F_{n'n'-1} & E_{n'}-\lambda'+F_{n'n'} \end{pmatrix} \end{pmatrix}, \tag{45}$$

where the submatrices correspond to the diagonalization indicated in (44). In each of these submatrices the off-diagonal term is of the form

$$F_{mn}(E)=g^2P\int dE'\frac{V_{mE'}V_{E'n}}{E-E'}, \tag{46}$$

where g is the electron-hole coupling constant and $V_{mE'}$ is the scattering amplitude due to the dynamically screened Coulomb interaction gV from the resonant state m to the scattering state E' belonging to the same channel. Replacing the energy denominator in (46) by a mean energy it is seen that

$$(F_{mn})^2\lesssim F_{mm}F_{nn}.$$

As the coupling constant g is increased the off-diagonal part of the exciton photon self-energies, neglecting interband scattering, is of comparable importance as the diagonal part in determining the binding energy of the excitons.[5]

(ii). The effect of the partial breakdown of the GRPA contributes further to configuration interaction and corresponds to interband scattering. This is taken into account by the terms $\Lambda_{\mu\mu'}+\Lambda_{\mu\mu'}{}^\dagger$ abbreviated in (45) to $\Lambda_{\mu\mu'}$. Consequently the new resonant energies are further shifted from E_ν and are obtained on diagonalizing the energy matrix (45). The fact that $\Lambda_{\mu\mu'}+\Lambda_{\mu\mu'}{}^\dagger$ mix the two channels is easily seen from (25):

$$\Lambda_{\mu\mu'}(E)=g^2P\int dE'\frac{V_{\mu E'}W_{E'\mu'}}{E-E'}.$$

The new resonant energies due to the real part of

the total self-energies of the exciton-photon field, for the sake of brevity, are again denoted by E_ν, it being clearly understood that the influence of interband scattering has been included.

The effects of the energy shifts due to configuration interaction are invoked to explain the resonant energies in the xenon spectra as observed experimentally by Baldini. Two striking facts are observed. Firstly one would expect that the binding energies of the $1s\,\Gamma(\frac{3}{2})$ and $1s\,\Gamma(\frac{1}{2})$ excitons should be about the same. In actual fact the binding energy of the $1s\,\Gamma(\frac{1}{2})$ exciton is 0.6 eV less than that of the $1s\,\Gamma(\frac{3}{2})$ exciton. Such a big difference cannot be explained solely on the basis of the contribution of the hole to the effective mass.[5]

Secondly from our line shape analysis, we saw that the $L(\frac{3}{2})$ peak is composite. The splitting of the excitons is 0.21 eV and that of their parent interband edges 0.5 eV. It is beyond the scope of this paper to compute the exciton splitting from the band splitting.[28] However, splittings for various L excitons λ_L, and their parent interband edges λ_B, for various alkali halide[4] crystals and solid xenon are shown in Fig. 9. The line represents a least-squares fit to the alkali-halide data. Because the saddle-point exciton wave packets, while concentrated near L, are spread throughout the Brillouin zone, in general $\lambda_L \lesssim \lambda_B$. In alkali halides the effects corresponding to configuration interaction are weak. However, these effects are greatly enhanced for xenon where $\lambda_L < \lambda_{B/2}$.

It is our contention that both these striking facts may be attributed to the effects of configuration interaction. Figure 10 is a schematic plot of the effects of configuration interaction as the electron-hole coupling constant g is switched on. The higher members of the $\Gamma(\frac{1}{2})$ series interact with the $L(\frac{3}{2})$ excitons so that they

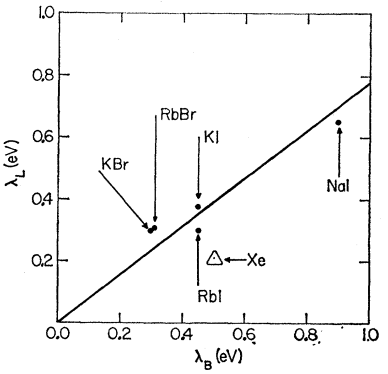

FIG. 9. Illustration of the effect of configuration interaction in xenon on the splitting of the L peaks. The quantities λ_L and λ_B represent the splitting of the L excitons and their parent interband edges, respectively. The values for the alkali halides are obtained from Phillips (Ref. 4). The exciton splitting of 0.21 eV for xenon is obtained from our theoretical analysis.

mutually repel each other. This repulsion depends on the proximity of the various levels. So the higher $\Gamma(\frac{1}{2})$ excitons are depressed whilst the $L(\frac{3}{2})$ excitons are raised. The exciton corresponding to $L_{4,5}^-(\frac{3}{2}) \rightarrow L_1$ is called the lower $L(\frac{3}{2})$ exciton and that corresponding to $L_{6u}^-(\frac{3}{2}) \rightarrow L_1$ the upper $L(\frac{3}{2})$ exciton. The lower $L(\frac{3}{2})$ exciton nearest the $\Gamma(\frac{1}{2})$ series is raised more than the upper $L(\frac{3}{2})$ exciton. Also there is configuration interaction between the metastable excitons $L(\frac{3}{2})$ and $L(\frac{1}{2})$. The $L(\frac{1}{2})$ exciton is raised whilst the $L(\frac{3}{2})$ excitons are depressed. The upper $L(\frac{3}{2})$ exciton is depressed more than the lower $L(\frac{3}{2})$ one. The net result of the configuration interaction can be obtained quantitatively only by diagonalization of the energy matrix (45). However Fig. 10 depicts the results qualitatively. As the electron-hole coupling constant g is increased the result of the

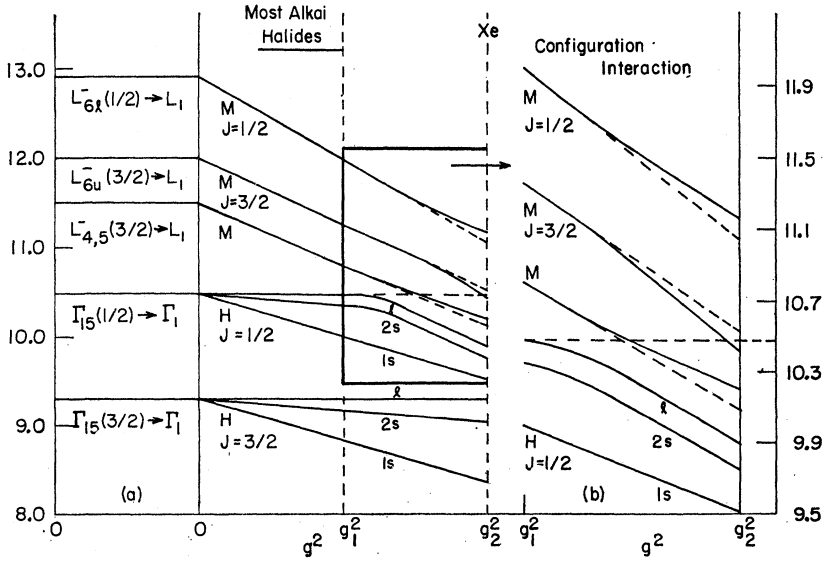

FIG. 10. (a) Schematic plot of the coherent exciton spectrum in xenon for $l=0$ as a function of the electron-hole coupling constant g, illustrating the effects of configuration interaction. The coupling constant for the alkali-halide excitons g_1, due to large dielectric constants, is smaller than that for the xenon excitons g_2. Hence the effects of configuration interaction are weaker in alkali halides than in xenon. M and H label the metastable and hydrogenic excitons respectively. (b) Details of the region of strong configuration interaction in xenon. The dashed lines indicate what the resonant energies would have been in the absence of configuration interaction while the solid lines indicate the actual resonant energies of the excitons.

[28] J. Hermanson, Phys. Rev. (to be published).

configuration interaction is to depress the I $(\frac{1}{2})$ and the upper $L(\frac{3}{2})$ excitons. The lower $L(\frac{3}{2})$ and $L(\frac{1}{2})$ excitons are raised. The limit of the $\Gamma(\frac{1}{2})$ series is depressed by 0.60 eV whilst the upper and lower $L(\frac{3}{2})$ excitons are pushed together so that they are now spin-orbit split by only 0.21 eV.

Apart from shifting the resonant energies, another effect of configuration interaction is to change the relative oscillator strengths of the various excitons.

The oscillator strengths of a hydrogenic series[12] normally vary like n^{-3} and for s states depend upon $|\phi(0)|^2$. This is corroborated by our theoretical analysis of solid xenon (see Table I) for the $\Gamma(\frac{3}{2})$ hydrogenic series. In this case the effects of configuration interaction are feeble and do not distort the series. However, the oscillator strengths of the $2s$ and the limit of the $\Gamma(\frac{1}{2})$ series are comparable and equal about $\frac{1}{4}$ of the $1s$ oscillator strength. This can be explained on the basis of configuration interaction with the $L(\frac{3}{2})$ excitons. Due to this interaction, the wave packets of the higher members of the $\Gamma(\frac{1}{2})$ series will no longer be taken entirely from the vicinity of Γ. Rather there will be admixtures from all points in the Brillouin zone, the effect of which will be to enhance $|\phi(0)|^2$ and augment the oscillator strengths of these higher members. Hence the effect of the configuration interaction has been to distort the wave functions also so that the members of the $\Gamma(\frac{1}{2})$ "hydrogenic" series no longer obey the n^{-3} rule in their oscillator strengths.

7. CONCLUDING REMARKS

We have refined the random phase approximation (RPA) formulation of the dielectric response of solids[8–11] to include resonance as well as scattering states. Our generalized random phase approximation differs from the conventional RPA because it includes interference terms and does not merely add the intensity of the resonance to the background scattering intensity.[2,13]

In analyzing the line shape of resonances it is important to distinguish between resonances which lie below or above the fundamental absorption edge. In the former case there is no background intensity in the absence of (dissipative) impurity or phonon scattering. However, at least a small amount of dissipative scattering is required to transfer energy from the exciton-photon field to the lattice, i.e., cause actual absorption.[29,30] This scattering will produce a weak background, and the resonance lines will interfere with the background. Then $|q_\nu|$ will be large, and the asymmetry will be apparent only near the bottom of the resonance. For such strong resonances superimposed on weak backgrounds the resonance-continuum self-energy effects that we have discussed are difficult to observe.

A question which naturally arises is that of the relationship of our model for the line shapes below threshold to that of Toyozawa.[2,13] In Toyozawa's theory the line shapes, below the absorption threshold, are discussed in terms of exciton-phonon self-energies. Second[2]-order or higher[13] order perturbation theory is used (see Appendix) and the interference terms coming from a pair of different intermediate states are rearranged so that each resonance becomes asymmetric and the so-called additivity rule is obtained. An antiresonance is obtained which subtracts from the background. The latter is calculated from the tails of the other resonances. As Toyozawa points out,[13] this approach to background scattering does not restrict the depth of antiresonance to values such that the total absorption be always greater than zero. In fact this has to be imposed as a subsidiary condition. Our model does not need such a condition because the absorption is always a positive-definite quantity. Another attractive feature of the approach given here is the emphasis on reaction channels, with a given resonance or antiresonance confined to one channel. This places further restrictions on antiresonant behavior.

Above the direct absorption threshold in general asymmetries and antiresonances are derived from exciton-photon self-energies. (The exciton-phonon self-energies usually play a small role,[31,32] just as indirect absorption is usually neglected in this region.) Below the threshold one finds narrow resonances separated by broad antiresonant minima. Above threshold the state of affairs is reversed: the tops of the resonances are broad, but in the well-annealed specimens the antiresonances are narrow and sharp.

In analyzing resonant spectra in the fundamental absorption spectrum we have introduced a number of parameters Γ_α, γ_α, q_α for each resonance α. One problem would be to determine each of these parameters from microscopic calculations. This is an interesting problem which appears to be soluble for two-electron atomic resonances,[33,34] at least in a few simple cases.[35] In our case detailed knowledge of energy bands as well as a sophisticated treatment of hyperbolic energy surfaces would be required to determine these parameters.[36] We have preferred to regard these parameters as phenomenological quantities, and focus our attention on the line shape, particularly of antiresonances.

---

[29] Pekar points out the necessity of scattering or thermal decay of the exciton for real absorption. See Ref. 30.

[30] S. I. Pekar, Zh. Eksperim. i Teor. Fiz. **36**, 451 (1959) [English transl.: Soviet Phys.—JETP **9**, 314 (1959)].

[31] An exception is the hyperfine structure found near absorption edges or peaks in the ultraviolet reflectance spectra of many semiconductors due to exciton-induced multiphonon transitions. This point has been discussed by Phillips in Ref. 32.

[32] J. C. Phillips, Phys. Rev. Letters **10**, 329 (1963).

[33] R. P. Madden and K. Codling, Phys. Rev. Letters **10**, 51, 6 (1963); **12**, 106 (1964).

[34] J. W. Cooper, U. Fano, and F. Prats, Phys. Rev. Letters **10**, 518 (1963).

[35] E. E. Salpeter and M. H. Zaidi, Phys. Rev. **125**, 248 (1962).

[36] Although we do not calculate the intrinsic autoionization rates Γ_α, we mention that their small values ($\lesssim$0.03 eV for Γ excitons in Xe, $\lesssim$0.05 eV for L excitons in Xe and CdTe) are not unexpected because of the two-electron character of the autoionization processes. See Refs. 33, 34, and 35.

We have found that a multichannel formalism based on our GRPA is required to explain the narrow, sharp antiresonances. We have even been able to show that rather small channel mixing, corresponding to an interband scattering rate 0.01 as large as intraband scattering, gives a best fit to the experimental data. The line shape is sensitive to such small channel mixing because of interference effects.

An interesting by-product of our analysis is a discussion of configuration interaction of parabolic and hyperbolic (saddle-point) exciton resonances. Such configuration interaction represents a most intriguing microscopic problem for future study.

ACKNOWLEDGMENT

I wish to express my deep gratitude to Professor J. C. Phillips for having suggested the problem, and for his constant help and encouragement during all the phases of this work.

APPENDIX

Toyozawa has considered[13] the absorption using Van Hove's[37] resolvent formalism. The unperturbed Hamiltonian H_0 consists of the electron and phonon parts whilst the electron-phonon interaction gV is treated as a perturbation. Then a partial diagonal singularity is obtained for the interaction term:

$$\langle \lambda \mathbf{K} n | VA_1VA_2\cdots A_mV | \lambda' \mathbf{K}' n' \rangle = \delta(\mathbf{K}-\mathbf{K}')\delta_{nn'}F_1(\lambda\lambda',\mathbf{K},n)+F_2(\lambda\lambda',\mathbf{K}\mathbf{K}',nn').$$

Here $(\lambda,\mathbf{K})$ are the quantum numbers for the relative and translational motion of an electron-hole pair and the eigenvalues of the phonon system are specified by n. From this, using Van Hove's theorem, he obtained an integral equation for the decay matrix (see 3.16 of Ref. 13) and an expression for the absorption coefficient (4.3 of Ref. 13). The only interference effects that are obtained there are those that correspond to $\lambda\lambda'$ mixing since the irreducible part is only partially diagonal. Hence Toyozawa's formalism gives an additivity rule, but it does not take into account, in a self-consistent manner, the continuum scattering.

To see in detail why this is so, we consider the Hamiltonian matrix schematically:

$$\begin{pmatrix} \text{excitons} & \text{electron-phonon} \\ \text{electron-phonon} & \text{continuum} \end{pmatrix}.$$

The Van Hove formalism computes continuum contributions to the exciton block by treating the coupling through phonons by diagrammatic perturbation theory. In this way one calculates exciton self-energies, but a consistent treatment of continuum self-energies is required. Also required to compute the optical absorption is a parallel treatment of exciton and continuum oscillator strengths. If only the exciton oscillator strengths associated with the upper left-hand block are included phenomenologically, then one has still to obtain the continuum contribution—i.e., the background—corresponding to the lower right-hand block. By treating these contributions on an equal footing, our phenomenological approach guarantees their compatibility.

It may be noticed that in Fig. 6 and in Fig. 8 the high-energy side of the $\Gamma(\frac{3}{2})$ $1s$ exciton is much too asymmetric according to our model, which makes configuration averages and treats the tails of the excitons as if they were uniformly distributed spatially throughout the crystal. When the resonance is very strong and the background is weak this is probably a poor model. The line shape of exciton tails, which often follow Urbach's rule, can probably be better understood in terms of a self-trapping model. The exciton-phonon interaction can then be described in terms of localized configuration coordinates, according to Toyozawa.[38] This gives a more symmetric line shape and weaker antiresonances. On the other hand, those exciton interactions with the lattice that involve nonlocalized phonon modes, and which determine a background absorption which is nearly spatially uniform, should be treated by our method. In practice it may be difficult to separate the asymmetries of resonances below the edge into parts caused by localized phonons and parts caused by interference with a nonlocalized background. Resonance asymmetries above the absorption edge are almost certainly dominated by the latter.

[37] L. Van Hove, Physica **21**, 901 (1955).

[38] Y. Toyozawa, The Institute for Solid State Physics, The University of Tokyo, Tokyo, Report No. A**119**, 1964 (unpublished).